



Two- and three-dimensional natural and mixed convection simulation using modular zonal models in buildings

Etienne Wurtz^{a,*}, Jean-Michel Nataf^b, Frederick Winkelmann^b

^a *L.E.P.T.A.B, Université de La Rochelle, 17000 La Rochelle, France*

^b *Lawrence Berkeley National Laboratory, Berkeley, CA 94720, U.S.A.*

Received 6 December 1997; in final form 18 May 1998

Abstract

We demonstrate the use of the zonal model approach, which is a simplified method for calculating natural and mixed convection in rooms. Zonal models use a coarse grid and use balance equations, state equations, hydrostatic pressure drop equations and power law equations of the form $m = C\Delta P^n$. The advantages of the zonal approach and its modular implementation are discussed. The zonal model resolution of nonlinear equation systems is demonstrated for three cases: a 2-D room, a 3-D room and a pair of 3-D rooms separated by a partition with an opening. A sensitivity analysis with respect to physical parameters and grid coarseness is presented. Results are compared to computational fluid dynamics (CFD) calculations and experimental data. © 1998 Elsevier Science Ltd. All rights reserved.

Nomenclature

C permeability of the border between two zones [$\text{m s}^{-1} \text{Pa}^{-n}$]
 c_p heat capacity [kJ kg^{-1}]
 g gravitation constant [m s^{-2}]
 h height of a zone [m]
 h_{cv} surface exchange coefficient [$\text{W m}^{-2} \text{K}^{-1}$]
 l width of the border [m]
 M molar mass [kg]
 n flow natur characteristic parameter [s]
 P_0 pressure at the bottom of a zone [Pa]
 P_{middle} pressure in the middle of a zone [Pa]
 P_{top} pressure at the top of a zone [Pa]
 q_m mass flow [kg s^{-1}]
 $q_{m_{\text{inf}}}$ horizontal mass flow below the neutral point [kg s^{-1}]
 $q_{m_{\text{sup}}}$ horizontal mass flow above the neutral point [kg s^{-1}]
 $q_{m_{\text{vert}}}$ vertical mass flow rate of air [kg s^{-1}]
 q_{sink} mass flow to sinks [kg s^{-1}]
 q_{source} mass flow from source [kg s^{-1}]
 R perfect gas constant
 S surface of the border [m^2]

T absolute temperature [K]
 z height in a zone [m]
 z_n height of the neutral point [m].

Greek symbols

Φ_{horiz} horizontal heat flux [W m^{-2}]
 Φ_{sink} heat transfer to sink [W s^{-1}]
 Φ_{source} heat transfer from sources [W s^{-1}]
 Φ_{vert} vertical heat flux [W m^{-2}]
 ρ density [kg m^{-3}].

1. Introduction

The study of air flow in buildings is important for the evaluation of energy consumption, moisture and pollutant transport, and comfort. The physical phenomena at work are natural or forced convection.

Natural convection has been extensively studied from theoretical, numerical and experimental points of view. The theory considers laminar boundary layer similarity or non-similarity solutions, as for example in [15, 19, 40, 60]. Many results have been obtained on standard

* Corresponding author

problems, such as the ‘window problem’, in which natural convective flow occurs in a room with both hot and cold surfaces [14, 21, 22, 45, 47]. Variations in geometry have been addressed ([56, 62]). Real rooms, with or without forced convection, have for the most part been analysed using CFD, as in [26, 51, 55], and, with obstacles, in [27]. CFD has also been used for large rooms and whole buildings [13, 41, 61].

The major difficulty with CFD, especially in three dimensions, is that the calculations are very slow and require large amounts of memory. Some methods, like the multi-grid method [43], mitigate the problem but still require significant computational resources. Furthermore, the sheer size of the output requires considerable effort in post-processing and visualization.

Other methods bypass the fluid mechanics equations. An example is the one-air-node approach, which is often used for multizone air flow calculations ([23, 29]). The main drawback of this approach is the coarseness of the results. This method, when coupled with CFD as is sometimes done ([30, 55]), suffers from the inherent difficulties of the CFD approach.

An intermediate approach is needed that allows the flow pattern inside a room to be determined without the computational investment of CFD. One such approach is the ‘zonal method’, which is adapted to a building’s domain characterised by big volumes and where the comfort can be described with only a few numbers of outputs.

2. The zonal method

2.1. Previous work

The zonal method, which is not new, is based on heat and mass balance equations in macroscopic volumes. Added to this is a relationship between mass flow and pressure difference. The zonal method should not be confused with models used to calculate air flow between rooms [23, 29, 52, 63, 64].

Initial work on the zonal method emphasised how to partition the computational domain in two dimensions [31, 38, 42]. A systematic attempt to use the zonal method with power law equations on arbitrary geometries in two dimensions is described in [17], in which convergence problems were encountered and the results did not agree well with measurements.

The present work treats the 3-D simulation case, with natural or mixed convection. Results were validated against CFD calculations and measurements. In addition we coupled 3-D zonal models with models for thermal comfort, wall conduction and directed flow. Other studies [53, 54] have considered the 3-D case, but did not couple to other models and were not validated.

2.2. Presentation of the method

In the 3-D zonal method the room air is partitioned into 3-D zones. Adjacent zones exchange mass and energy. The following mass and energy balance equations apply to each zone:

$$\Sigma q_m + q_{\text{source}} - q_{\text{sink}} = 0$$

$$\Sigma \Phi + \Phi_{\text{source}} - \Phi_{\text{sink}} = 0$$

where Σq_m is the sum of mass flows across the interfaces of the zones, q_{source} is the mass flow from sources in the zone, q_{sink} is the mass flow to sinks in the zone, $\Sigma \Phi$ is the sum of heat transfers through the interfaces of the zone, Φ_{source} is the heat transfer from sources in the zone and Φ_{sink} is the heat transfer to sinks in the zone.

We assume that a zone has uniform temperature and density and that the pressure at the middle of a zone obeys the perfect gas law:

$$P_{\text{middle}} = \rho \frac{R}{M} T$$

where ρ is the density, R the perfect gas constant, M the molar mass and T the absolute temperature. The pressure at height z above the bottom of a zone is given by

$$P = P_0 + \rho g z$$

where P_0 is the pressure at the bottom of the zone.

Assuming that the zones are rectangular parallelipeds with edges oriented along the coordinate axes, the gist of the zonal model lies in the following equations:

The elementary mass flow rate dq_m is:

$$dq_m = c\rho(\Delta P)^n ds$$

The pressure differential at level is:

$$\Delta P = \Delta P_0 - \Delta\rho g z$$

The level z_n of the neutral axis is:

$$z_n = \frac{\Delta P_0}{\Delta\rho g}$$

For vertical interfaces, depending on the position of the neutral axis z_n and the value of ρ , we have to break down the flow rate q_m into two flows $q_{m_{\text{sup}}}$ and $q_{m_{\text{inf}}}$

$$q_{m_{\text{sup}}} = Cl\rho(\Delta\rho g)^n \frac{(h - z_n)^{n+1}}{n+1}$$

$$q_{m_{\text{inf}}} = Cl\rho(\Delta\rho g)^n \frac{(z_n)^{n+1}}{n+1}$$

The flow exchanged becomes:

$$q_m = q_{m_{\text{sup}}} + q_{m_{\text{inf}}}$$

For horizontal interfaces, the pressure differential is uniform at the border level and there is only one flow rate:

$$q_{m_{\text{vert}}} = C\rho S(P - P_{\text{top}})^n.$$

Here P_{top} is the pressure at the top of the zone, q_m are mass flows, C is an empirical constant equal to $0.83 \text{ m s}^{-1} \text{ Pa}^{-n}$ [38] (a parametric study has shown the validity of this parameter), l is the width of a zone, h is the height of a zone, n is a fractional exponent, Δ is a difference operator between two horizontally adjacent zones, z_n is the height of the neutral point (the point at which pressures on either side of the interface between two zones are equal), ρ is the volumetric mass, vert is an index for vertical mass flow, m_{sup} an index for horizontal mass flow above the neutral point and m_{inf} is an index for horizontal mass flow below the neutral point. It is assumed that flow is incompressible and pressure drop is hydrostatic.

Energy fluxes are calculated using the following equations, which are valid for temperatures typically found in buildings and which, for now, neglect humidity:

$$\Phi_{\text{horiz}} = q_{m_s} c_p T_s + q_{m_e} c_p T_e$$

$$\Phi_{\text{vert}} = q_{m_{\text{vert}}} c_p T_{\text{vert}}$$

where Φ denotes a heat flux, horiz stands for horizontal and vert for vertical. Here q_{m_s} denotes mass flow leaving the zone and q_{m_e} denotes mass flow entering the zone. T_s is the temperature of the air leaving the zone, which is the same as the zone temperature, and T_e the temperature of the air entering the zone. T_{vert} is the zone temperature for vertical flow out of the zone and is the adjacent zone temperature for vertical flow into the zone. We use a sign convention such that a mass flow is positive when the flow is in the positive direction of an x , y or z axis, and negative when in the negative direction of an axis.

If the standard area represents a portion of a partition, a convective exchange takes place which can be modeled by a coefficient h_{cv} . The heat flow then reads:

$$\Phi_{\text{cv}} = h_{\text{cv}} S (T - T_w)$$

where T_w is the temperature of the wall.

2.3. Physical considerations

Several remarks can be made about the validity of the model. (1) Coarse grids and high temperature gradients may make uniform temperature in a zone a poor assumption. (2) Temperature and velocity boundary layers are not accounted for. (3) The hydrostatic pressure approximation is valid only for flows with parallel streamlines. (4) Only one neutral point per vertical interface between zones is allowed, which, depending on the gridding, affects the qualitative behavior of the solution. (5) Along the lines of [17], the Bernoulli equation used amounts to assuming that kinetic energy is fully dissipated within the bounds of a single zone, and so does not apply to plumes or jets that span two or more zones, as rediscovered in [53].

2.4. Numerical considerations

An obvious property of the above equations is their nonlinearity. The $n = 0.5$ exponent is a source of par-

ticular numerical difficulty since it is well known that standard Newton–Raphson iteration (without relaxation) does not converge when there are square-root dependencies. An additional source of trouble is that, because they depend on flow direction, the equations must be piecewise defined, even if they are formally unified, as in [28]. Finally, 3-D problems generally lead to a fairly large number of equations. This ‘dimensional curse’ also exists for zonal models. For example, some problems analyzed with zonal methods require resolving more than 2000 equations.

2.5. Insight on a simplified case: the window problem

2.5.1. Two-zone case

We consider now the application of the zonal model to the well-known ‘window’ problem in which a two-dimensional rectangular cavity is heated by a warm isothermal wall on the left and cooled by a cold window (in our case, actually a cold isothermal wall) on the right. The ceiling and floor are assumed to be adiabatic. For this configuration the room air density will, on average, be smaller on the left, and the resulting circulation will be clockwise. We divide the room into two zones, one on the left and one on the right. Because of buoyancy effects we expect the air to flow from left to right at the top of the room and from right to left at the bottom. We assume that there are no mass sources or sinks, that the convection at the walls is Newtonian and that $n = 0.5$. The solution will be given in terms of the widths, l_1 and l_2 , of the left and right zones, respectively, the height, h of the zones, the convective heat transfer coefficients, h_h and h_c of the hot and cold walls, respectively, the hot and cold wall temperatures, t_h and t_c , respectively, and the total room air mass, m .

2.5.2. Algebraic simplification in the two-zone case

Simplification by substitution produces a nonlinear system of two equations and two unknowns. The simplification was done automatically using the MACSYMA computer algebra program [8]. The simplification algorithm that was used is described in [9]. Basically, the algorithm transforms the equation system into a graph and then uses graph theory to find a small number of iteration variables.

During the simplification process MACSYMA asks questions, such as whether the neutral point is located above the height of a zone or not, which zone has the higher specific air mass, ρ , etc. The answers to these questions are unique, even though, in some cases, an intermediate calculation of the sign of expressions is required (such as whether $h_c(t_c - t_1) + h_h(t_h - t_1) > 0$). The resulting simplified system of equations is also unique.

The unknowns remaining after simplification by MACSYMA are t_2 and ρ_2 , the air temperature and density, respectively, of the right-hand zone. However,

this simplification is not complete, due to the presence of fractional powers, which lead to alternative solutions that MACSYMA cannot resolve. Further simplification can be carried out, producing one (very nonlinear) equation in ρ_2 that can be solved numerically. Note that if fractional power simplification is turned on in MACSYMA, two equations, in ρ_2 and z_n , result.

Results from the computer algebra reduction agree with numerical results obtained with an independent numerical solver, called SPARK, which is described in Section 3. However, the final equations are too unwieldy to use, and there are two of them, in terms of moderately interesting variables. We would be more interested in only one final equation (since resolution of one nonlinear equation, however complicated, can be done efficiently and safely), possibly in terms of one mass flow, q_m , for example (since what we are mainly interested in is the heat transfer and the mass circulation). The conclusion of interest of this model is the global heat transfer from the left wall to the right wall.

Reordering the set of equations and reformulating the pressure power law equations to express them with the ρ 's solved for, one can actually get down to one equation with residual unknown ρ_2 . The (large) surviving equation gives by the MACSYMA implementation of the reduction algorithm is given in the Appendix.

This equation has the form $ax_3 = (x-c)^2$ where a and c are positive, where x is $\rho_2 - \rho$ the reduced cold zone air density, where

$$c = \frac{l_1(T_{\text{hot}} - T_{\text{cold}})}{l_1 T_{\text{cold}} + l_2 T_{\text{hot}}} \rho$$

is proportional to the temperature difference, and where

$$a = \frac{2c_p^2 g h k^2 (l_1 - l_2)^3 \rho^2 (h_{\text{hot}} T_{\text{hot}} + h_{\text{cold}} T_{\text{cold}})^2}{36 h_{\text{cold}}^2 h_{\text{hot}}^2 l_1^2 (l_1 T_{\text{cold}} + l_2 T_{\text{hot}})^2}$$

The order of magnitude of c is

$$\frac{1}{300},$$

and of a is 5×10^5 .

It can be shown graphically that this 3rd order equation has a real solution between 0 and X , where

$$X = \frac{l_1(T_{\text{hot}} - T_{\text{cold}})}{l_1 T_{\text{cold}} + l_2 T_{\text{hot}}} \rho$$

Furthermore, we know that the solution can be expressed in closed form by radicals (since we are dealing with a 3rd order polynomial). Solving the equation using the following input values

[hhot = 4, hcold = 4., h = 3., l1 = 2., l2 = 3., l3 = 3., mair = 0.029, r = 8.314. rho = 1.205, cp = 1004., g = 9.81, k = 0.83, that = 303., tcold = 283.];

gives 1.206244948428609 as the value of the only one of three roots that is real. This is acceptable and expected (the air is denser on the cold side). Numerical back propa-

gation (substitution) of this symbolic solution to the other variables of interest leads to:

$$\begin{aligned} \text{RHO2} &= 1.206244948428609 \\ \text{RHO1} &= 1.203755051571391 \\ \text{T1} &= 293.3027135161184 \\ \text{T2} &= 292.6972864838816 \\ \text{QMLow} &= 0.3828828788442727 \\ \text{PHI} &= 232.7348756131578 \\ \text{P1} &= 101219.9750313746 \\ \text{P2} &= 101219.9750902376 \\ \text{P10} &= 101237.6882869585 \\ \text{P20} &= 101237.7249846537 \end{aligned}$$

By inspection we see that these results are reasonable. In particular, the middle pressures are equal, which is expected from the finding that the neutral point is exactly at mid height.

Comparison with a numerical solution of the same problem in slightly different units (degrees Celsius and reduced pressures instead of degrees Kelvin and absolute pressures), using zonal models and the SPARK environment, yields

$$\begin{aligned} \text{RHO2} &= 1.206010\text{E}+00 \\ \text{RHO1} &= 1.203521\text{E}+00 \\ \text{T1} &= 2.030105\text{E}+01 + 273 = 293.3 \\ \text{T2} &= 1.969943\text{E}+01 + 273 = 292.7 \\ \text{QMLow} &= 3.827173\text{E}-01 \\ \text{PHI} &= 2.326966\text{E}+02 \\ \text{P1} &= -6.948886\text{E}+01 + 101325 = 101255 \\ \text{P2} &= -6.948892\text{E}+01 + 101325 = 101255 \\ \text{P20} &= -5.173599\text{E}+01 + 101325 = 101374 \\ \text{P10} &= -5.177318\text{E}+01 + 101325 = 101374 \end{aligned}$$

The pressures differ by about 35 Pa. However, the symbolic simulation assumes a perfectly tight room, which the numerical simulation does not and so the value of pressure depends on outside conditions.

Another (small) cause of discrepancy is that the power law used in the symbolic simulation is multiplied by a default density, whereas the numerical simulation uses the upstream density.

On the other hand, the temperatures, the mass flows and the heat transfers agree almost perfectly.

2.5.3. Qualitative observations in the two-zone case

Qualitatively, we see that ρ_2 decreases when a increases (i.e., when the height or permeability coefficient increases, or when the convective heat transfer at the wall decreases). On the other hand, ρ_2 increases when c increases.

Also, we see that ρ_2 increases when the wall-to-wall temperature difference, $T_{\text{hot}} - T_{\text{cold}}$, increases. This is because c is proportional to $T_{\text{hot}} - T_{\text{cold}}$ and a is slowly varying since it is the square of a homographic function.

Finally, since a is large, it can be shown graphically that the physical root of $ax^2 = (x-c)^2$ is close to the

root of $ax^3 = c^2$, or $x = c^{2/3}a^{-1/3}$. This trend confirms and sharpens the above statements. For example, $\rho_2 - \rho$ varies like $h^{-1/3}$.

2.5.4. Global heat transfer in the two-zone case

With computer algebra we automatically obtain the set of substitutions needed to calculate the other unknowns. The variable of interest, the global heat transfer, Φ , is obtained from the following sequence of substitutions:

$$\begin{aligned} \phi &= H * HHOT * L * THOT - H * HHOT * L * T1 \\ QMSUP &= QMLOW \\ T1 &= (HHOT * THOT * + HCOLD - * \\ COLDHCOLD * T2)/HHOT \\ T2 &= (CP * HHOT * QMLOW * THOT + (CP * \\ HCOLD * QMLOW + H * HCOLD * HHOT * L) * \\ TCOLD)/(CP * HHOT + CP * H * COLDD) * \\ QMLOW + H * HCOLD * HHOT * L) \\ QMLOW &= -(2 * SQRT(G) * K * L * RHO * \\ SQRT(RHO2 - RHO1) * SQRT(H - ZN) * ZN - 2 * \\ SQRT(G) * H * K * L * RHO * \\ \#SQRT(RHO2 - RHO1) * SQRT(H - ZN))/3 \\ ZN &= H/2 \\ RHO1 &= -(L2 * RHO2 + (-L2 - L1) * RHO)/L1 \end{aligned}$$

We note that the neutral point for this simple case is always at mid height. The final equation for Φ is:

$$\begin{aligned} \phi &= H * HHOT * L * THOT - H * L * (-HCOLD * \\ (CP * SQRT(G) * \hat{H}(3/2) * HHOT * K * L * RHO * \\ SQRT((\#L2 * RHO2 + (-L2 - L1) * RHO)/ \\ L1 + RHO2) * THOT/(3 * SQRT(2)) + (CP * SQRT(G) \\ * \hat{H}(3/2) * HCOLD * K * L * \#RHO * SQRT((L2 * \\ RHO2 + -L2 - L1) * RHO)/L1 + RHO2))/(3 * \\ SQRT(2)) + H * HCOLD * HHOT * L) * \\ TCOLD)/(S \# QRT(G) * H [mao0](3/2) * (CP * \\ HHOT + CP * HCOLD) * K * L * RHO * SQRT((L2 * \\ RHO2 + (-L2 - L1) * RHO)/L1 + RHO2) \#/(3 * \\ SQRT(2)) + H * HCOLD * HHOT * L) + HHOT * \\ THOT + HCOLD * TCOLD) \end{aligned}$$

The ratio Nu (Nusselt number) of Φ to the purely conductive flux

$$h \frac{k - \{air\} \frac{T - \{hot\} - T - \{cold\}}{1 - 1 + 1 - 2}}{is}$$

$$\begin{aligned} &SQRT(G) SQRT(H) (CP HCOLD HHOT K L2 + CP \\ &HCOLD HHOT K L1) RHO SQRT ((L2 + L1) \\ &RHO2 + (-L2 - L1) RHO)/(SQRT(G) SQRT(H)(CP \\ &HHOT + CP HCOLD) K KAIR RHO SQRT ((L2 - L1) \\ &RHO2 + (-L - L1) RHO) + 3 SQRT(2) HCOLD \\ &HHOT KAIR SQRT(L1)) \end{aligned}$$

This is a rational function in $\sqrt{\rho_2 - \rho}$. Further simplification leads to:

$$Nu = \frac{\frac{l_1 + l_2}{k_{air}}}{\left(\frac{1}{h_{hot}} + \frac{1}{h_{cold}}\right) + \frac{3\sqrt{2} \sqrt{\frac{l_1}{l_1 + l_2}}}{c_p \sqrt{ghk} \frac{1}{\rho \sqrt{\rho_2 - \rho}}}}$$

For the problem under consideration we obtain

$$Nu = \frac{1}{0.0021 + \frac{0.0000023}{\sqrt{\rho_2 - 1.205}}}$$

which is about 465.

We see that the larger value of ρ_2 (due, for example, to an increase in temperature difference), produces a large value of Nu .

2.5.5. Comparison of the two-zone case with theory

In laminar natural convection (see e.g., [15]), Nu depends on the Rayleigh number, Ra_h , according to

$$Nu = 0.364 \frac{l_1 + l_2}{h} Ra_h^{1/4}.$$

A rough evaluation using $Ra_h = 107000000h^3$, $\Delta T = 57780000000$, an approximation valid at those temperatures, yields $Nu = 356$. Thus, Nu increases as $h^{3/4}$ and as $\Delta T^{1/4}$. For turbulent natural convection Nu varies as $\Delta T^{1/3}$ since

$$Nu = 0.65 Gr_h^{1/3} \left(\frac{h}{l_1 + l_2}\right)^{-1/9}$$

according to the Jakob correlation. Numerical application to our problem yields $Nu = 304$.

Thus, the coarse-grained two-zone zonal model overestimates the ratio of convective to conductive heat transfer by 30–50%.

The zonal model applied to two continuous zones exhibits a qualitatively appropriate behavior: an increase in h or ΔT does increase Nu if the other parameters are held constant.

We should also take into account the temperature dependence of the wall heat transfer coefficients, h_{hot} and h_{cold} to better account for the temperature dependence of Nu . Nu depends on the harmonic mean of the wall heat transfer coefficients, which, in turn, go as $Ra^{1/4}$. Thus, the qualitative behavior of the zonal model, even in the simple two-zone case, is consistent with the theoretical and experimental natural convection if the wall heat transfer coefficients are chosen appropriately.

2.5.6. Two-zone case with inlet air

A generalization of the two-zone problem is to allow air to flow in (at the left, for example) at a specified rate.

Assuming that circulation still exists, i.e., that the inlet flow is small enough not to disturb the flow pattern, we can again reduce the overall system to two equations in unknowns ρ_2 and z_n . One equation is a second-order polynomial in $\sqrt{\rho_2 - \rho}$ that can be eliminated by solving for ρ_2 , leaving a single equation in z_n . However, this equation contains large, nonpolynomial expressions. Thus little can be said on the parameter dependency of its solutions, unlike in the previous case.

3. Numerical implementation: the SPARK environment

3.1. Presentation and history

The Simulation Problem Analysis and Research Kernel (SPARK) is a modular environment that automates writing code for systems of nonlinear equations. It was developed for building science but is applicable to other fields. It is related to simulation environments like TK!Solver [39], TRNSYS [57], CLIM2000 [16], IDA [11], and Allan.Simulation [25].

Some key features of SPARK are:

- It has a front end that allows the user to build complex simulations by connecting smaller elements that are objects (single equations) or macro-objects (equation subsystems). It shares this feature with TRNSYS, CLIM2000 and Allan.Simulation.
- Using graph-theoretic techniques, it reduces the size of the equation system by automatically determining a small set of iteration variables for which the other unknowns can be solved. This step can be viewed as ‘smart’ elimination of variables. SPARK’s Newton–Raphson solver works on the reduced equation set and, after convergence, the remaining unknowns are solved for. This is a unique feature. Allan.Simulation, for example, generates code that inverts the full Jacobian matrix.
- Its output is a C program that is automatically compiled and executed. This program accepts user-specified input at run time and is computationally efficient because it iterates on a reduced set of variables.
- Passing from a simulation problem to a design problem (i.e., having unknowns become inputs and inputs become unknowns) is simply a matter of keyword exchange in SPARK.

Originally written in 1986 for steady state problems [12], it was extended in 1989 to handle transient problems by adding time integrator objects [58]. Recent enhancements include:

- Automatic generation of objects from equations expressed symbolically ([49, 59]).
- Strong component decomposition to reduce execution time [18].

- User control of solution method to enhance convergence.

3.2. Implementation of the zonal model

Implementation of zonal models in SPARK is straightforward. The main object classes correspond to the zones and to the interfaces between zones. A zone class consists of the balance equations for the zone, the pressure drop equation and the perfect gas law. An interface class consists of the neutral point calculation and the relationship between mass flow and pressure difference.

These classes are instantiated as many times as needed to define the simulation. For example, if a 3-D room is divided into eight parallelepipeds (two in each of the x , y and z directions), there will be eight zone objects and 36 interface objects (12 zone-to-zone interfaces and 24 zone-to-surface interfaces). In the general 3-D case, if the x , y and z axes are divided into L , M and N sections, respectively, there will be LMN zone objects and $3(LM + MN + LN)$ interface objects. In 2-D there will be LM zone objects and LM zone-to-zone interface objects and $2LM$ zone-to-surface interface objects.

After instantiation, the objects are linked, i.e., the variables shared by objects are identified. Then the objects and their linked variables are stored in a file that specifies the overall problem and its inputs.

3.3. Efficiency

The efficiency of a simulation environment depends on the time and resources needed to solve a simulation problem. SPARK obtains a near-optimal simplification of the problem, without loss of precision, by automatically reducing the number of iteration variables. The reduction can be more than 10-fold, which corresponds to a roughly 1000-fold decrease in Jacobian inversion time. SPARK also makes it easy to create a simulation from scratch by using symbolic processing to create the simulation building blocks (equation objects) from equations written by the user [49]. In the present work even the linking of objects was automated [50].

Table 1 shows the efficiency of SPARK reduction.

To facilitate interpretation of results, a graphical post-processor was written to visualize temperatures and air flows.

4. The 2-D ‘window’ problem

4.1. Description

A 2-D, 6×2.4 m shallow enclosure has its left wall maintained at 12°C , its right wall at 20°C , and its floor and ceiling at 15°C . The surface heat transfer is assumed to be linear in surface-to-air temperature difference, with con-

Table 1
Efficiency of SPARK reduction for the different cases presented

	Number of subvolumes	Average time of simulation (min)	Number of variables	Number of equations after reduction	Memory required (Mo)
2-D case	36	3	432	108	4.7
3-D case	64	12	2240	192	11.0
Minibat	108	23	3744	324	17.0

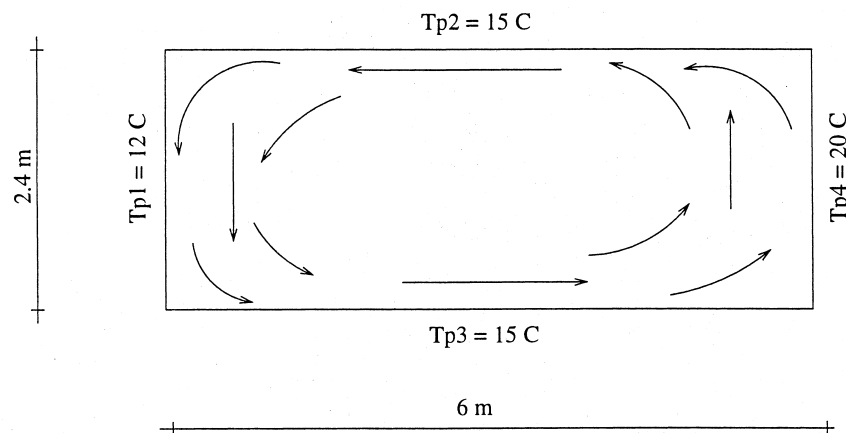


Fig. 1. Natural convective flow in the 2-D 'window' model.

vective heat transfer coefficients, h , of 4.1, 1.0 and 5.7 $\text{W m}^{-1} \text{K}^{-1}$ at the walls, floor and ceiling, respectively [38].

Two different grids were used for the zonal model, 3×3 and 6×6 , which yield 108 and 432 equations, respectively. After reduction in SPARK, there were 18 and 72 equations, respectively. The iteration variables chosen were the temperature and midpoint pressure of each zone.

4.2. Numerical validation

The calculated flow field is shown qualitatively in Fig. 1. The expected circulation pattern is observed, i.e., downward flow across the cold wall and upward flow across the warm wall. The results were compared to runs using the CFD code Fluent [38], which is based on the finite volume method and uses uniform gridding, logarithmic velocity profiles near surfaces, and the $k-\epsilon$ turbulence model.

Figures 2 and 3 show that the air temperatures for the zonal and CFD models are similar. The maximum difference between the models is 8% along the mid-room horizontal axis and 10% along the mid-room vertical axis.

The zonal model's temperature distribution is more 'conductive' than the CFD distribution because the zonal model is diffusive (assumes perfect mixing) and ignores thermal boundary layers.

The agreement between the air flow velocity results (Figs 4 and 5) is less satisfactory than for the temperatures but still acceptable.

The error is above 10% close to the floor and ceiling. Again, the zonal model does less well close to the walls since it does not account for boundary layer effects.

4.3. Sensitivity analysis

We see that changing the grid from 3×3 to 6×6 in the window problem barely changes the results, which indicates that a coarse grid is adequate.

We also tested the sensitivity of the model to the permeability coefficient, C , and to the wall heat transfer coefficients, h . The results are given in Figs 6 and 7, which show how the temperature distribution changes with C , and in Fig. 8, which shows how the velocity distribution changes with C . We see that air temperature and velocity are fairly insensitive to C and that the best results are obtained with the commonly accepted value of 0.83 [46].

We also found that the results are insensitive to h (not shown). We conclude that a zonal model with coarse gridding gives acceptable results for the 2-D window problem even with uncertainties in the values of permeability and surface heat transfer coefficients.

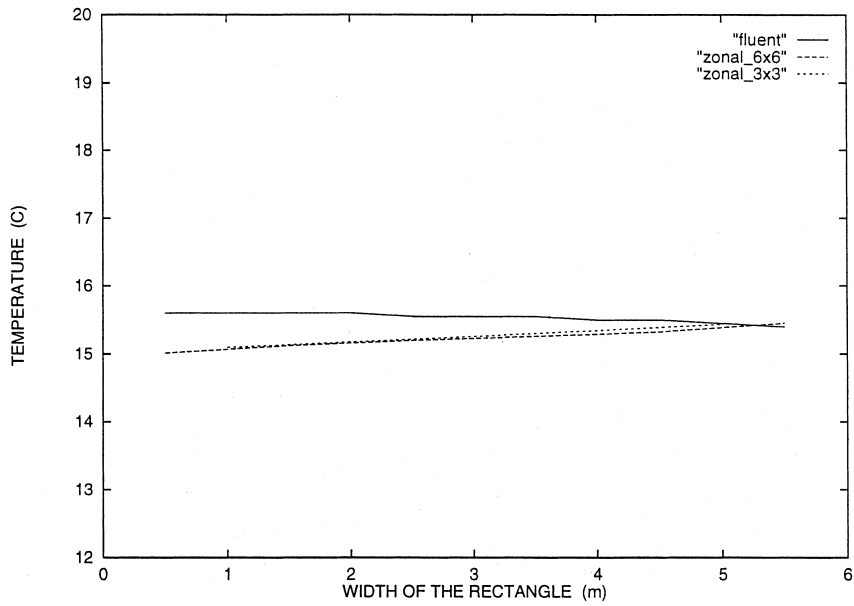


Fig. 2. 2-D 'window' problem: horizontal distribution of air temperature at mid-height predicted by the zonal model (for 3×3 and 6×6 gridding) and the Fluent CFD calculation.

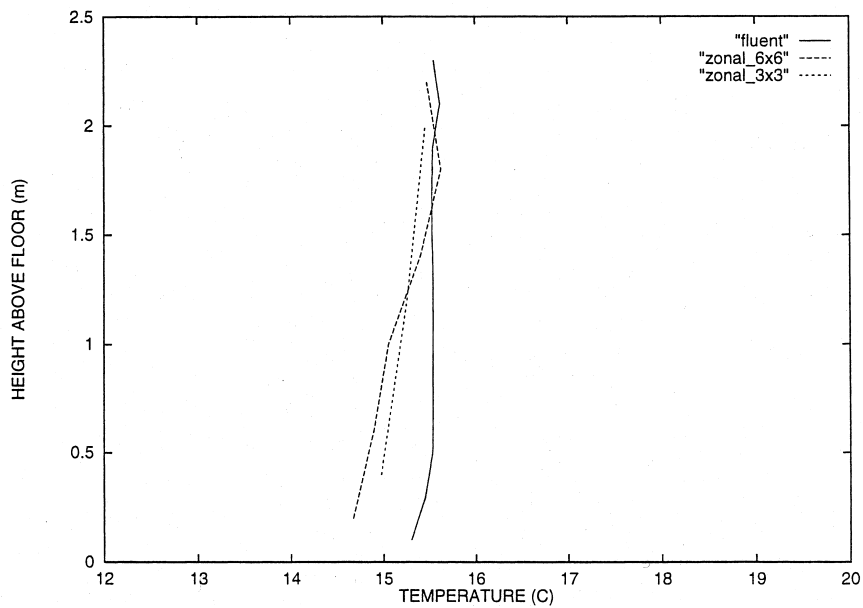


Fig. 3. 2-D 'window' problem: vertical distribution of air temperature at mid-room predicted by the zonal model (for 3×3 and 6×6 gridding) and the Fluent CFD calculation.

5. The 3-D parallelepiped

5.1. Description

A 3-D $2.6 \times 3.6 \times 2.55$ m cell has the left wall maintained at 25.5°C , the right wall at 32°C , the ceiling at

26°C and the other walls at 24.5°C . The convective heat transfer coefficients at the walls are the same as in the 2-D case.

We chose a grid that was $4 \times 4 \times 4$, which produced 2240 equations. With an exponent of 1 in the mass flow equations, SPARK reduced this to 128 equations (a 16 to

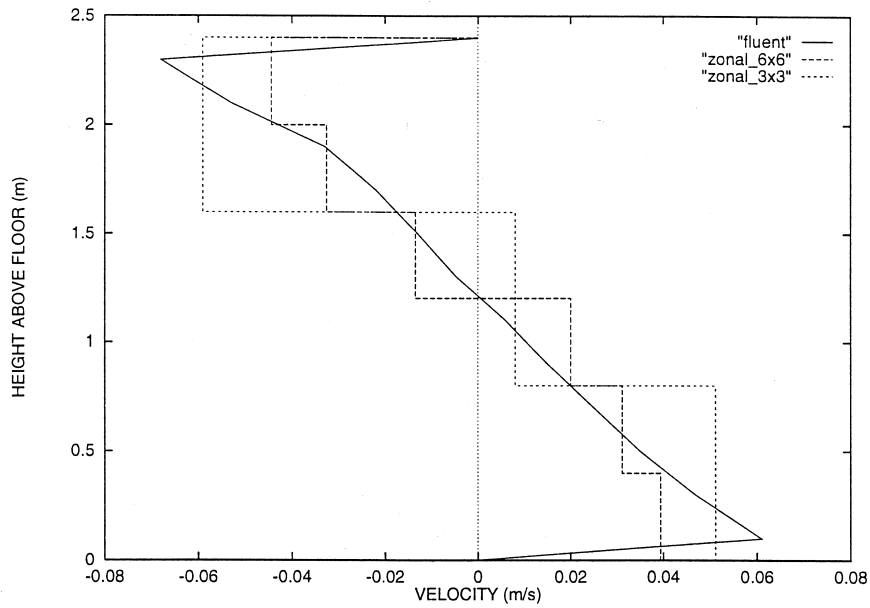


Fig. 4. 2-D ‘window’ problem: vertical distribution of horizontal air velocity predicted by the zonal model (for 3×3 and 6×6 gridding) and the Fluent CFD calculation.

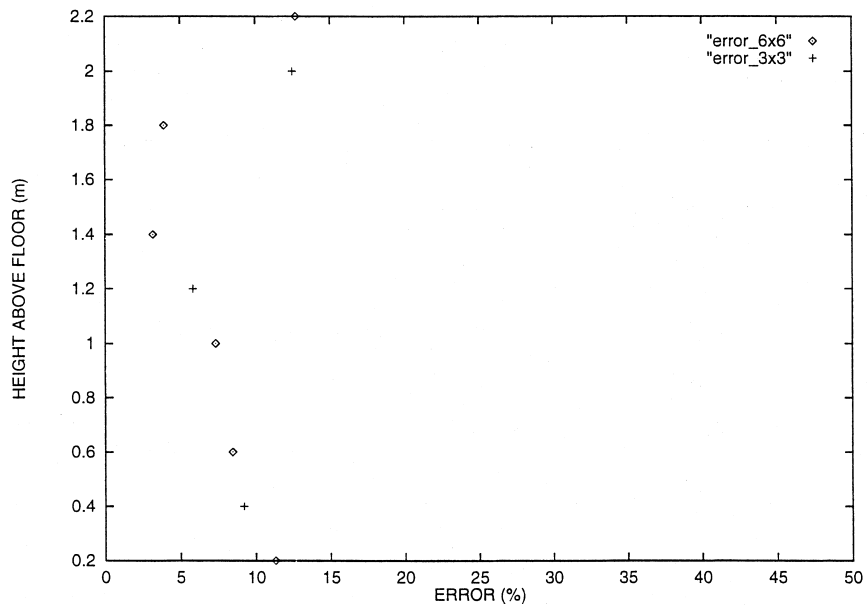


Fig. 5. 2-D ‘window’ problem: percent difference in horizontal air flow velocity vs height above floor between zonal model (for 3×3 and 6×6 gridding) and Fluent CFD calculation.

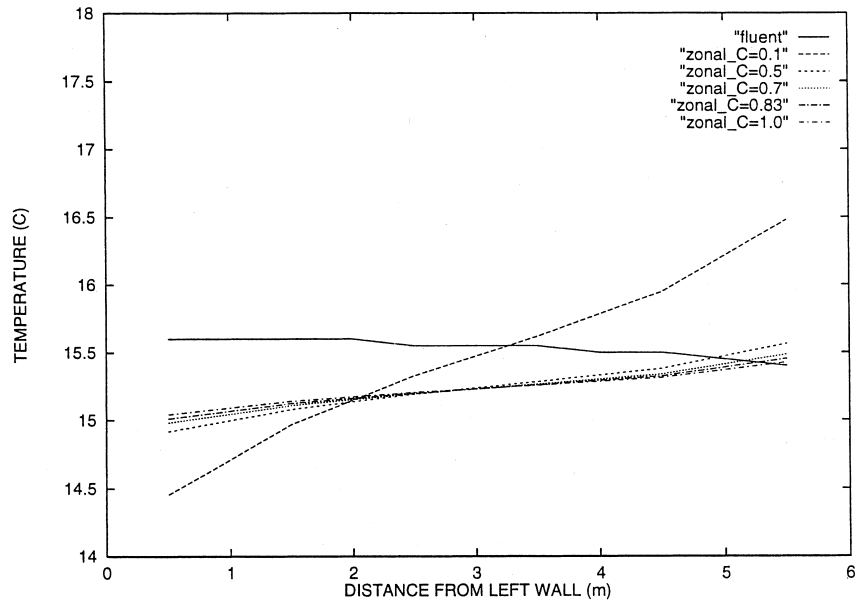


Fig. 6. 2-D 'window' problem: sensitivity to permeability coefficient of the horizontal distribution of air temperature as determined by the zonal model. Prediction of the Fluent CFD model is shown for comparison.

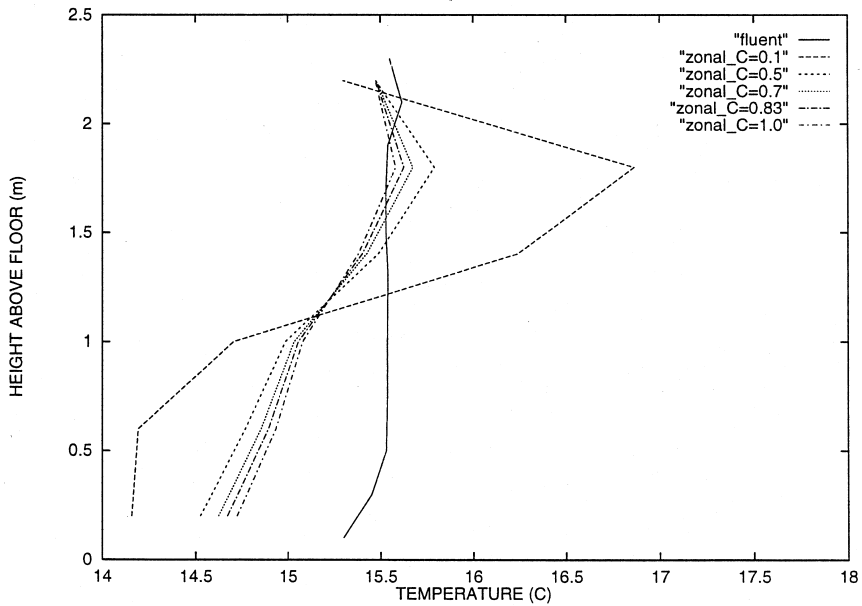


Fig. 7. 2-D 'window' problem: sensitivity to permeability coefficient of the vertical distribution of air temperature as determined by the zonal model. Prediction of the Fluent CFD model is shown for comparison.

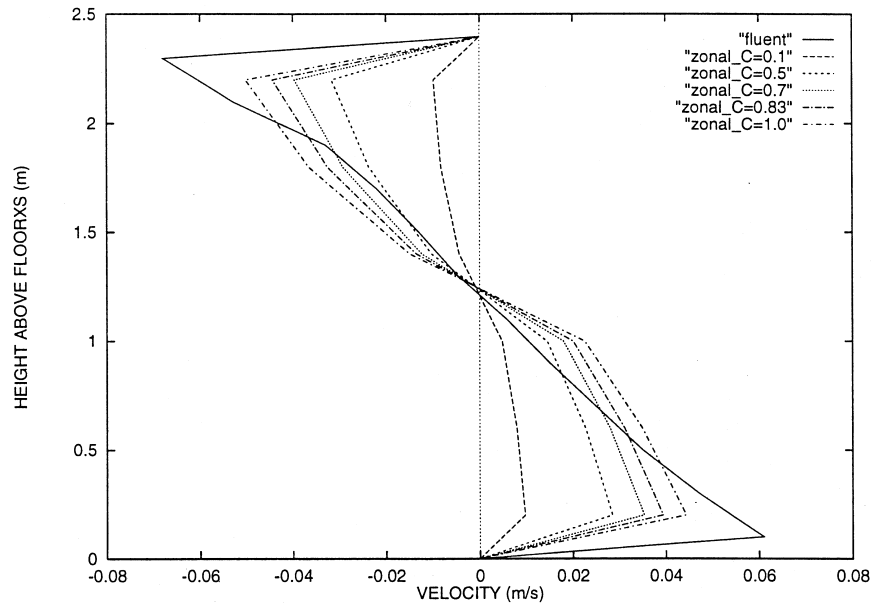


Fig. 8. 2-D 'window' problem: sensitivity to permeability coefficient of the horizontal distribution of vertical air velocity. Prediction of the Fluent CFD model is shown for comparison.

1 reduction). Convergence was achieved with a Newton–Raphson relaxation coefficient of 0.5, and by choosing initials values that were close to the final solution.

5.2. Validation

The zonal model results were validated numerically and by comparing with experimental results. Numerical validation was done using the Fluent CFD code. A temperature comparison is shown in Figs 9 and 10, and a velocity comparison in Fig. 11. The zonal model temperatures are close to the CFD results, and lie between the CFD and measured values. The largest differences between zonal model and measurements, which is about 2°C, occurs near the floor, where the air is cooler and diffusion is smaller. As expected, the difference between the zonal model and measured air velocity is largest near the walls. We found better agreement (not shown) by using smaller zones near the walls.

6. The minibat cell

6.1. Presentation of the problem

To test the zonal approach on a more complex problem, we modeled the 'Minibat Cell', a test structure at INSA (Institut National des Sciences Appliquées) in Toulouse, France. This 6.2 × 3.1 × 2.5 m cell is divided into a warm room and a cold room by a partition that

has a 0.77 m wide × 1.83 m high open doorway. The left wall is maintained at 28.0°C, the right wall at 22.5°C, the ceiling at 25.0°C on the warm side and 24.81°C on the cold side, the floor at 24.58°C and the other walls at 24.63°C.

We used a 6 × 3 × 6 grid, which led to 3744 equations. SPARK reduced this to 216 equations (a 17 to 1 reduction).

6.2. Validation

The air temperature distributions calculated by the zonal model on the warm and cold sides are shown in Figs 12 and 13. The air velocity distribution in the doorway is shown in Fig. 14. For comparison, these figures also show measured data and the predictions of the StarCD CFD program, which is based on a finite-volume method.

The zonal model's temperature results are satisfactory. They fall, for the most part, between the measured and the CFD values. As in the previous test case, the highest discrepancy occurs near the floor. The overall agreement with measured and CFD results is somewhat better on the warm side of the cell.

The zonal model currently predicts the qualitative behavior of the air flow in the doorway, but, quantitatively, there are differences up to 25% relative to the measurements. Flows are generally overestimated in the doorway, although the neutral point is correctly calculated. This indicates that better agreement would be

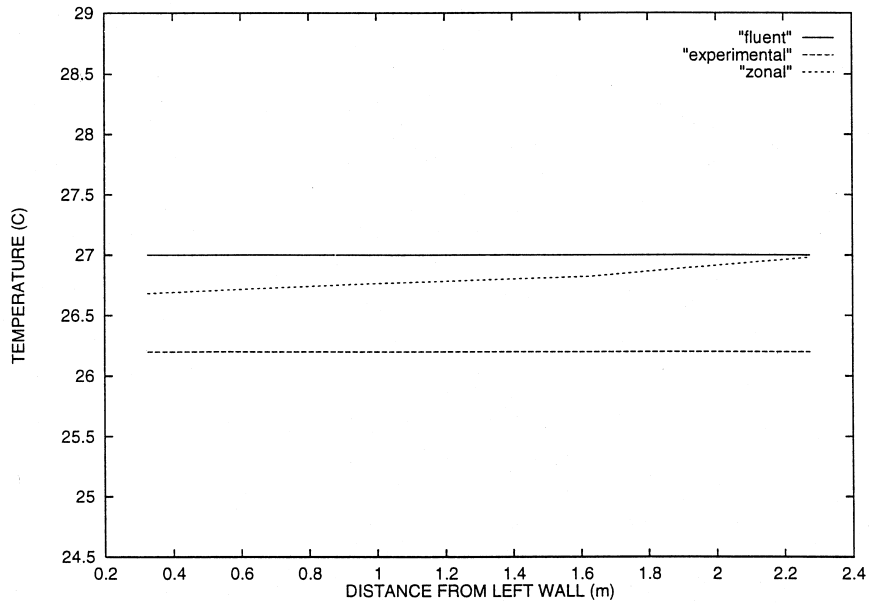


Fig. 9. Comparison of the measured horizontal distribution of the air temperature at mid-height with the predictions of the 3-D zonal model and the Fluent CFD calculation.

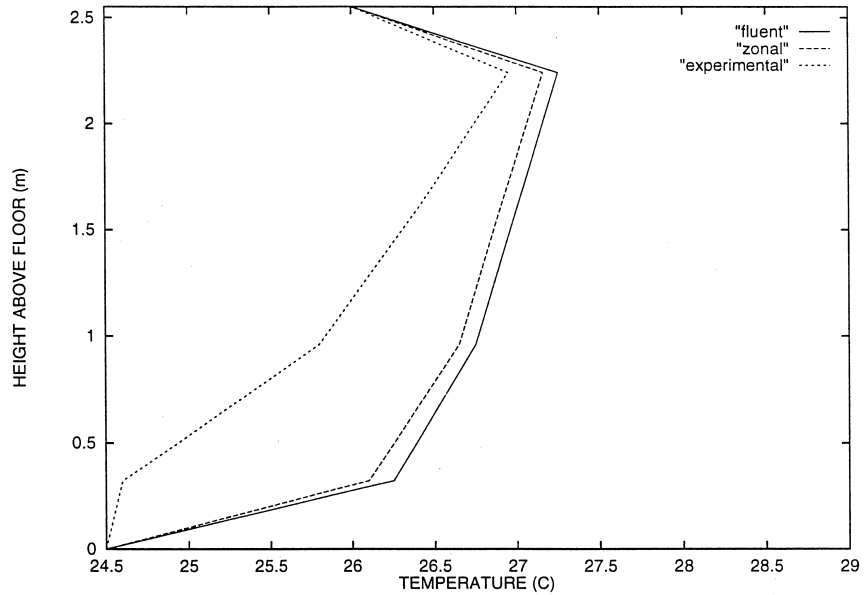


Fig. 10. Comparison of the measured vertical distribution of air temperature at room center with the predictions of the 3-D zonal model and the Fluent CFD calculation.

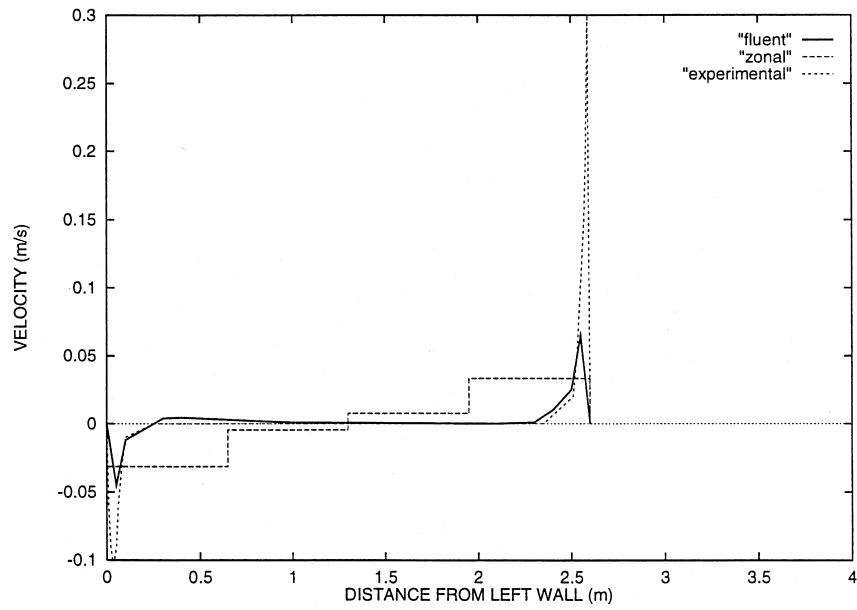


Fig. 11. Comparison of the measured horizontal distribution of the vertical air velocity at mid-height with predictions of the zonal model and the Fluent CFD calculation.

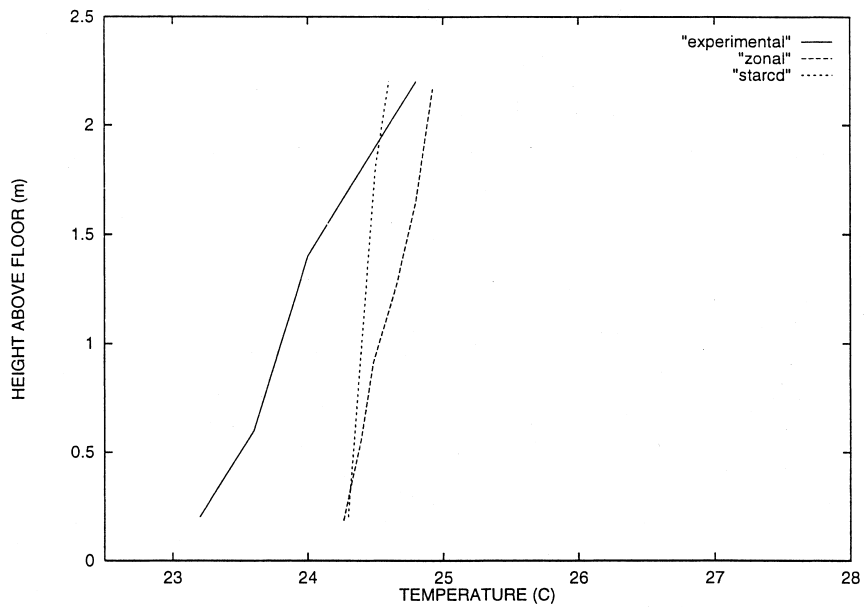


Fig. 12. Comparison of the measured vertical distribution of air temperature on the cold side of the Minibat cell with predictions of the zonal model and the Star CD CFD calculation.

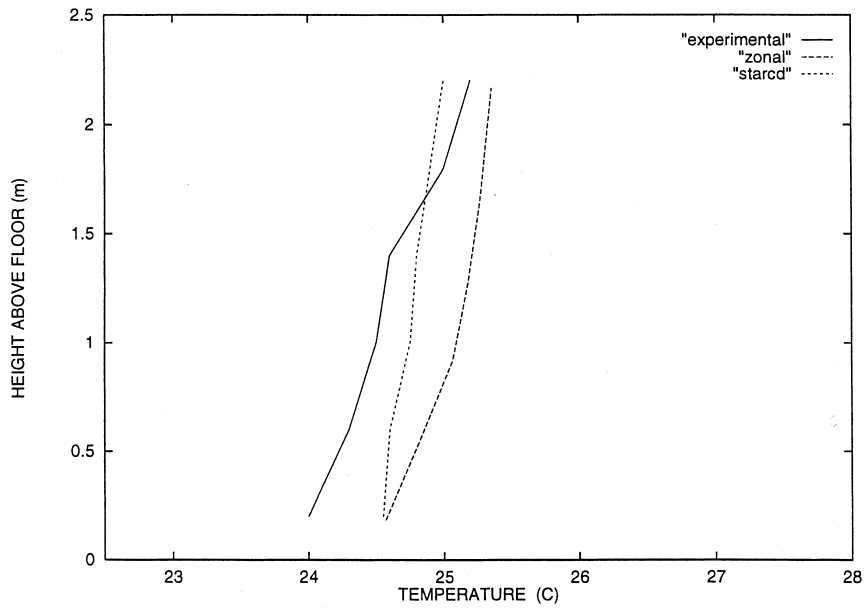


Fig. 13. Comparison of the measured vertical distribution of air temperature on the warm side of the Minibat cell with predictions of the zonal model and the Star CD CFD calculation.

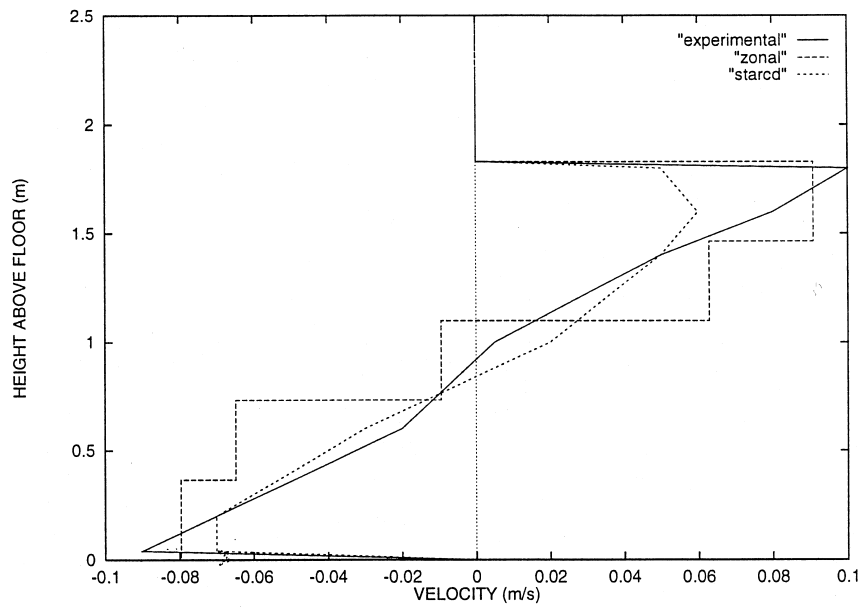


Fig. 14. Comparison of the measured vertical distribution of horizontal air velocity in the doorway of the Minibat cell with predictions of the zonal model and the Star CD CFD calculation. Air moving from right to left (from the cold side to the warm side) is considered to have positive velocity.

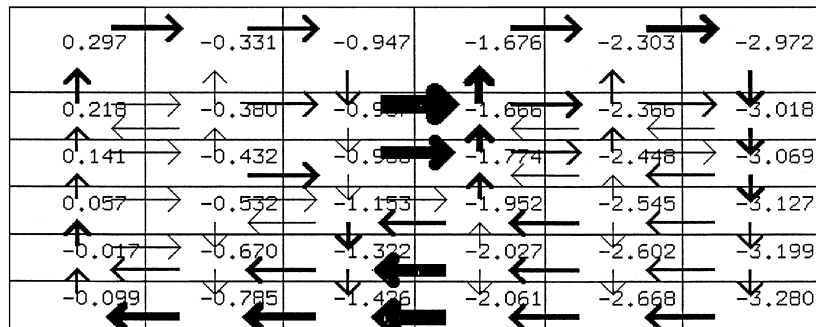


Fig. 15. Comfort analysis based on coupling of Fanger model and zonal model: predicted mean vote in vertical-midplane zones of the Minibat cell. The arrows show air flow between zones.

obtained by reducing the permeability coefficient in the opening [48].

7. Coupling to external models

Having demonstrated the overall reliability of zonal models, at least for simple rectangular geometries, we demonstrate in this section modularity and reusability in object-based simulation by coupling the zonal model with a comfort model.

7.1. Comfort model

We consider a simple, classic comfort model—the Fanger model [1]—which is expressed as

$$CT = H - E - R - C$$

$$PMV = [0.303e^{-0.036M} + 0.028] \times CT.$$

Here, CT is the state of thermal comfort, which is determined by occupant activity level, H , evaporation rate, E , radiative heat loss, R , and convective heat loss, C . PMV is the predicted mean vote, for which a zero value of 0 corresponds to feeling comfortable, a positive value to feeling too warm and a negative value to feeling too cold.

Because of the modularity of the SPARK environment, all that was needed to couple the comfort and zonal models was to add the Fanger equations to the zone equations. The results of solving the resulting equation set for the Minibat Cell are shown in Fig. 15.

7.2. Wall-to-air coupling

Air flow models should be coupled to realistic wall models. The modularity of the SPARK object-based approach allows wall models to be easily created using the ‘modal’ method [24]. In this method the conduction equations for complex geometries are solved in full and

the significant modes are determined. This reduces the complexity of the model with little loss of accuracy.

We incorporated the wall conduction flux from the modal approach into the general energy balance equation for the air zones adjacent to the walls. Given the external conditions, the SPARK solver then determined the surface temperatures as well as the distributions of inside air temperature and air flow.

7.3. Coupling to a hydronic cooling system

The zonal model was also coupled to an independently developed SPARK simulation of a hydronic radiant cooling system in which the heat transfer to the room air was originally modeled assuming a single air node, i.e., assuming a uniform air temperature [20]. This coupling was accomplished in a straightforward fashion and led to a more accurate model in which the heat transfer from the cooled surfaces to the air took into account the spatial variation of air temperature.

7.4. Coupling to plumes and jets

The main weakness of zonal models is that they cannot properly represent air jets (from diffusers, for example) or plumes (which are common around heaters), since in these models jets and plumes are (incorrectly) assumed to be fully dissipated in the zone in which they originate. One way around this limitation is to replace zones that contain a jet or plume with a specific jet or plume object. To investigate this possibility we considered the case of a 3-D $4.75 \times 3 \times 2.5$ m room that had a heater next to a cold wall. A $6 \times 6 \times 4$ grid was used in which the zonal models for the three zones above the heater were replaced with a plume object. We found in this case that a pure zonal model without a plume object gave unacceptable results (for example, there was an unphysical horizontal diffusion immediately above the heater). However, when

a plume object was used a physically reasonable air flow pattern was observed.

8. Conclusion and perspectives

We have shown that, for simple rectangular geometries, the zonal method gives reasonably accurate air flow and air temperature results even in 3-D cases (for which convergence problems are usually encountered when other methods are used). Zonal models are easier to incorporate in modular simulation environments than are CDF models and are much faster executing. Also, we need only global information to calculate comfort in a building and so do not require all the information given by CFD codes. It was difficult to compare execution times because FLUENT needed manual intervention to converge for free convection. However, further work is needed to establish guidance for optimal partitioning of rooms into zones. In particular, it should be determined whether partitioning can or should be based on the expected flow pattern. It would also be of interest to extend the zonal method to consider moisture and pollutant transport.

Acknowledgement

This work was partially supported by the Assistant Secretary for Energy Efficiency and Renewable Energy, Office of Building Technologies, Building Systems and Materials Division of the U.S. Department of Energy, under contract No. DE-AC03-76SF00098.

Appendix

Equation given by MACSYMA implementation:

$$H/2 = (\text{SQRT}(G) * \text{SQRT}(H) * \text{SQRT}(L1) * \text{SQRT}((L2+L1)) * \text{RHO}2 * (-L2-L1) * \text{RHO}) * (((2 * \text{SQRT}(2) * C\#P * \text{HHOT} * K * L2 + 2 * \text{SQRT}(2) * CP * \text{HHOT} * K * L1) * R * \text{RHO} * \text{RHO}2 + (-2 * \text{SQRT}(2) * CP * \text{HHOT} * K * L2 - 2 * \text{SQRT}(2) * CP * \text{HHOT} * K * L1) * R * \text{RH}0\hat{2}) * \text{THOT} + ((2 * \text{SQRT}(2) * CP * \text{HCOLD} * K * L2 + 2 * \text{SQRT}(2) * CP * \text{HCOLD} * K * L1) * R * \text{RHO} * \text{RHO}2 + (-2 * \text{SQRT}(2) * CP * \text{HCOLD} * K * L2 - 2 * \text{SQRT}(2) * CP * \text{HCOLD} * K * L1) * R * \text{RH}0\hat{2}) * \text{TC}\#OLD + ((\text{SQRT}(2) * CP * G * H * \text{HHOT} + \text{SQRT}(2) * CP * G * H * \text{HCOLD}) * K * L2 + (\text{SQRT}(2) * CP * G * H * \text{HHOT} + \text{SQRT}(2) * CP * G * H * \text{HCOLD}) * K * L1) * \text{MAIR} * \text{RHO} * \text{RHO}2 + ((-\text{SQRT}(2) * CP * G * H * \text{HHOT} - \text{SQRT}(2) * CP * G * H * \text{HC}\#OLD) * K * L2 + (-\text{SQRT}(2) * CP * G * H * \text{HHOT} - \text{SQRT}(2) * CP * G * H * \text{HCOLD}) * K * L1) * \text{MAIR} * \text{RHO} * \text{RHO}2 + (12 * \text{HC}\#OLD * \text{HHOT} * L1 * L2 * R * \text{RHO}2 + (-12 * \text{HCOLD} * \text{HHOT} * L1\hat{2}) * R * \text{RHO}) * \text{THOT} + 12 * \text{HCOLD} * \text{HHOT} * L1\hat{2} * R * \text{RHO}2 * \text{TCOLD} + (6 * G * H * \text{COLD} * \text{HHOT} * L1 * L2 + 6 * G * H * \text{HCOLD} * \text{HHOT} * L1\hat{2}) * M\#AIR * \text{RHO}2 + (-6 * G * H * \text{HCOLD} * \text{HHOT} * L1 * L2 - 6 * G * H * \text{HCOLD} * \text{HHOT} * L1\hat{2}) * \text{MAIR} * \text{RHO}) / (\text{SQRT}(G) * \text{SQ}\#RT(H) * \text{SQRT}(L1) * \text{SQRT}((L2+L1) * \text{RHO}2 + (-L2-L1) * \text{RHO}) * (((2 * \text{SQRT}(2) * CP * G * \text{HHOT} + 2 * \text{SQRT}(2) * CP * G * \text{HCOLD}) * K * L2 + (2 * \text{SQRT}(2) * CP * G * \text{HHOT} + 2 * \text{SQRT}(2) * CP * G * \text{HCOLD}) * K * L1) * \text{MAIR} * \text{RHO} * R\#HO2 + ((-2 * \text{SQRT}(2) * CP * G * \text{HHOT} - 2 * \text{SQRT}(2) * CP * G * \text{HCOLD}) * K * L2 + (-2 * \text{SQRT}(2) * CP * G * \text{HHOT} - 2 * \text{SQRT}(2) * CP * G * \text{HCOLD}) * K * L1) * \text{MAIR} * \text{RH}0\hat{2}) + (12 * G * \text{HCOLD} * \text{HHOT} * L1 * L2 + 12 * G * \text{HCOLD} * \text{HHOT} * L1\hat{2}) * \text{MAIR} * \text{RHO}2 + (-12 * G * \text{HCOLD} * \text{HHOT} * L1 * L2 - 12 * G * \text{HCOLD} * \text{HHOT} * L1\hat{2}) * \text{MAIR} * \text{RHO})$$

$$\text{CP} * \text{G} * \text{H} * \text{HCOLD}) * \text{K} * \text{L1}) * \text{MAIR} * \text{RHO} * \text{RHO}2 + (12 * \text{HC}\#OLD * \text{HHOT} * L1 * L2 * R * \text{RHO}2 + (-12 * \text{HCOLD} * \text{HHOT} * L1 * L2 - 12 * \text{HCOLD} * \text{HHOT} * L1\hat{2}) * R * \text{RHO}) * \text{THOT} + 12 * \text{HCOLD} * \text{HHOT} * L1\hat{2} * R * \text{RHO}2 * \text{TCOLD} + (6 * G * H * \text{COLD} * \text{HHOT} * L1 * L2 + 6 * G * H * \text{HCOLD} * \text{HHOT} * L1\hat{2}) * M\#AIR * \text{RHO}2 + (-6 * G * H * \text{HCOLD} * \text{HHOT} * L1 * L2 - 6 * G * H * \text{HCOLD} * \text{HHOT} * L1\hat{2}) * \text{MAIR} * \text{RHO}) / (\text{SQRT}(G) * \text{SQ}\#RT(H) * \text{SQRT}(L1) * \text{SQRT}((L2+L1) * \text{RHO}2 + (-L2-L1) * \text{RHO}) * (((2 * \text{SQRT}(2) * CP * G * \text{HHOT} + 2 * \text{SQRT}(2) * CP * G * \text{HCOLD}) * K * L2 + (2 * \text{SQRT}(2) * CP * G * \text{HHOT} + 2 * \text{SQRT}(2) * CP * G * \text{HCOLD}) * K * L1) * \text{MAIR} * \text{RHO} * R\#HO2 + ((-2 * \text{SQRT}(2) * CP * G * \text{HHOT} - 2 * \text{SQRT}(2) * CP * G * \text{HCOLD}) * K * L2 + (-2 * \text{SQRT}(2) * CP * G * \text{HHOT} - 2 * \text{SQRT}(2) * CP * G * \text{HCOLD}) * K * L1) * \text{MAIR} * \text{RH}0\hat{2}) + (12 * G * \text{HCOLD} * \text{HHOT} * L1 * L2 + 12 * G * \text{HCOLD} * \text{HHOT} * L1\hat{2}) * \text{MAIR} * \text{RHO}2 + (-12 * G * \text{HCOLD} * \text{HHOT} * L1 * L2 - 12 * G * \text{HCOLD} * \text{HHOT} * L1\hat{2}) * \text{MAIR} * \text{RHO})$$

In the above, the previous notations are capitalized. Thus H is the zone height h , G the acceleration of gravity g , $L1$ the length of the zone, etc.

This equation can be simplified by invoking various simplifiers from the MACSYMA functions. After simplification, the output is:

$$\text{SQRT}(2) * \text{CP} * \text{SQRT}(G) * \text{SQRT}(H) * \text{K} * \text{SQRT}((L1) * (L2+L1)\hat{3/2}) * \text{R} * \text{RHO} * (\text{RHO} * (\text{RHO}2 - \text{RHO})\hat{3/2}) * (\text{HHOT} * \text{THOT} + \text{HCOLD} * \text{TCOLD}) + 6 * \text{HCOLD} * \text{HHOT} * L1 * R * (L2 * \text{RHO}2 - L2 * \text{RHO} - L1 * \text{RHO}) * \text{THOT} + 6 * \text{HCOLD} * \text{HHOT} * L1\hat{2} * R * \text{RHO}2 * \text{TCOLD} = 0$$

which leads to the third order polynomial equation:

$$2 * \text{CP}^2 * G * H * \text{K}^2 * L1 * (L2+L1)\hat{3} * \text{RH}0\hat{2} * (\text{RHO}2 - \text{RHO})\hat{3} * (\text{HHOT} * \text{THOT} + \text{HCOLD} * \text{TCOLD})\hat{2} - (6 * \text{HCOLD} * \text{HHOT} * L1 * L2 * (L2 * \text{RHO}2 - L2 * \text{RHO} - L1 * \text{RHO}) * \text{THOT} + 6 * \text{HCOLD} * \text{HHOT} * L1\hat{2} * \text{TCOLD})\hat{2}$$

References

- [1] P.O. Fanger, Thermal Comfort, McGraw-Hill Book Company, New York, 1973.
- [2] J.L. Anderson, Cooling refreshment. Technical Report 21522, Lawrence Berkeley Laboratory, Berkeley, CA 94720, September 1987.
- [3] A. Bejan, Convection Heat Transfer. Wiley-Interscience, 1984.
- [4] H. Bouia, P. Dalicieux, Simplified modelling of air movements inside dwelling room, in: Proceedings of the Building Simulation '91 Conference, August 1991.
- [5] F. Buhl, E. Erdem, J.-M. Nataf, F. Winkelmann, E. Sowell,

- Recent improvements in SPARK: Strong component decomposition, multivalued objects and graphical interface. LBL Report LBL-33906, Lawrence Berkeley Laboratory, August 1993.
- [6] Gaz De France, Allan: Manuel de référence. Technical report, June 1992.
- [7] C. Inard, Contribution à l'étude du couplage thermique entre un émetteur de chauffage et un local. PhD thesis, Institut National des Sciences Appliquées de Lyon, July 1988.
- [8] MIT, MACSYMA Reference Manual, version 10, Cambridge, MA, 1983.
- [9] J.-M. Nataf, Algorithm of simplification of nonlinear equation systems, ACM SIGSAM Bulletin 26(1) (1992).
- [10] J.-M. Nataf, E. Wurtz, Application of the SPARK environment to 3d air flow problems, in: Proceedings of Building Simulations '93, Adelaide, Australia. International Building Performance Simulation Association, August 1993.
- [11] P. Sahlin, IDA, a modelling and simulation environment for building applications. Institute of Applied Mathematics, P.O. Box 26300, S-100 41, Stockholm, Sweden, 1988.
- [12] J.L. Anderson, A network definition and solution of simulation problems. Technical Report 21522, Lawrence Berkeley Laboratory, Berkeley, CA 94720, September 1987.
- [13] G.S. Barozzi, E. Nobile, M.S. Imbabi, A.C.M. Sousa, Scale models and CFD for the analysis of air flow in passively ventilated buildings, in: Proceedings of Building Simulation '91, Sophia-Antipolis, Nice, France (pp. 118–124). International Building Performance Simulation Association, 20–22 August, 1991.
- [14] F. Bauman, A. Gadgil, R. Kammerud, R. Greif, Buoyancy-driven convection in a rectangular enclosure; experimental results and numerical calculations. Technical Report LBL-10257, Lawrence Berkeley Laboratory, July, 1980.
- [15] A. Bejan, Convection Heat Transfer, John Wiley and Sons, 1984.
- [16] D. Bonneau, D. Covalet, D. Gautier, F.X. Rongere, Manuel de Prise en Main, CLIM2000, Version 0.0, 1989.
- [17] H. Bouia, P. Dalicieux, Simplified modelling of air movements inside dwelling room, in: Proceedings of Building Simulation '91, Sophia-Antipolis, Nice, France, International Building Performance Simulation Association, 20–22 August, 1991.
- [18] F. Buhl, E. Erdem, F. Winkelmann, E. Sowell, Recent improvements in SPARK: Strong component decomposition, multivalued objects and graphical interface, in: Proceedings of Building Simulation '93, Adelaide, Australia, International Building Performance Simulation Association, 16–18 August, 1993.
- [19] C.C. Chen, R. Eichhorn, Natural convection from a vertical surface to a thermally stratified fluid. Journal of Heat Transfer (1976) 446–451.
- [20] H.E. Feustel Corina Stetiu, F.C. Winkelmann, Development of a simulation tool to evaluate the performance of radial cooling ceilings. LBL and CIEE Report LBL-37300, UC-1600, Lawrence Berkeley Laboratory, June, 1995.
- [21] G. de Vahl Davis, Natural convection of air in a square cavity: a benchmark solution, Technical Report 1982/FMT/2, School of Mechanical and Industrial Engineering, University of South Wales, 1982.
- [22] G. de Vahl Davis, Natural convection of air in a square cavity: a benchmark numerical solution, International Journal for Numerical Methods in Fluids 3 (1983) 249–264.
- [23] H.E. Feustel et al., The comis infiltration model, in: Proceedings of Building Simulation '89, Vancouver, 1989.
- [24] B. Flament, L. Blanc-Sommereux, A. Neveu, A new technique for thermal modelling of buildings: the modal synthesis, in: Proceedings of Building Simulation '91, Sophia-Antipolis, Nice, France, International Building Performance Simulation Association, 20–22 August, 1991.
- [25] Gaz de France. Allan: Manuel de référence, allan.™.2.4.1. Technical report, Gaz de France, June, 1992.
- [26] A.J. Gadgil, On convective heat transfer in building energy analysis. LBL Report LBL-10900, Lawrence Berkeley Laboratory, May, 1980.
- [27] G. Gan, H.B. Awbi, D.J. Croome, Simulation of air flow in naturally ventilated buildings, in: Proceedings of Building Simulation '91, Sophia-Antipolis, Nice, France, International Building Performance Simulation Association, 20–22 August, 1991.
- [28] J. Hensen, J. van der Maas, A. Roos, Air and heat flow through large vertical openings, in: Proceedings of Building Simulation '93, Adelaide, Australia, International Building Performance Simulation Association, 16–18 August, 1993.
- [29] J.L.M. Hensen, J.A. Clarke, A simulation approach to the evaluation of coupled heat and mass transfer in buildings, in: Proceedings of Building Simulation '91, Sophia-Antipolis, Nice, France, International Building Performance Simulation Association, 20–22 August, 1991.
- [30] J.A. Clarke, W.M. Dempster, C. Negrao, The implementation of a computational fluid dynamics algorithm within the ESP-r system, in: Proceedings of Building Simulation '95, Madison, U.S.A., International Building Performance Simulation Association, August, 1995.
- [31] A.T. Howarth, The prediction of air temperature variations in naturally ventilated rooms with convective heating, Building Service Engineering Research and Technology 6(4) (1985) 169–175.
- [32] C. Inard, Contribution à l'étude du couplage thermique entre un émetteur de chauffage et un local, PhD thesis, Institut National des Sciences Appliquées de Lyon, July, 1988.
- [33] M. Konopasek, S. Jarayaman, Constraint and declarative languages for engineering applications: the tklsolver contribution, in: Proceedings of the IEEE 73(12), December 1985.
- [34] A.K. Kulkarni, H.R. Jacobs, J.J. Hwang, Similarity solution for natural convection flow over an isothermal vertical wall immersed in thermally stratified medium, International Journal of Heat and Mass Transfer 30(4) (1987) 691–698.
- [35] J. Lam, R. Yuen, T. Tau, Improvements to user-friendliness of a computational fluid dynamics (cfd) code for simulation of air movement in buildings, in: Proceedings of Building Simulation '93, Adelaide, Australia, International Building Performance Simulation Association, 16–18 August, 1993.
- [36] J. Lebrun, P. Ngendakumana, Air circulation induced by heating emitters and corresponding heat exchanges along the walls: test room results and modelling, in: Proceedings of Room Vent 1987, Stockholm, 1987.

- [37] Y. Li, S. Holmberg, L. Fuchs, Multi grid prediction of conjugate heat transfer and air flow in buildings, in: Proceedings of Building Simulation '93, Adelaide, Australia, International Building Performance Simulation Association, 16–18 August, 1993.
- [38] C. Inard, Contribution à l'étude du couplage thermique entre un émetteur de chauffage et un local. PhD thesis Institut National des Sciences Appliquées de Lyons, July, 1988.
- [39] M. Konopasek, S. Jarayaman, Constraint and declarative languages for engineering applications; the tk!solver contribution, in Proceedings of the IEEE, 73(12), December, 1985.
- [40] A.K. Kulkarni, H.R. Jacobs, J.J. Hwang, Similarity solution for natural convection flow over an isothermal vertical wall immersed in thermally stratified medium, International Journal of Heat and Mass Transfer 30(4) (1987) 691–698.
- [41] J. Lam, R. Yuen, T. Tau, Improvements to user-friendliness of a computational fluid dynamics (cfD) code for simulation of air movement in buildings, in: Proceedings of Building Simulation '93, Adelaide, Australia, International Building Performance Simulation Association, 16–18 August, 1993.
- [42] J. Lebrun, P. Ngendakumana, Air circulation induced by heating emitters and corresponding heat exchanges along the walls: test room results and modelling, in: Proceedings of Room Vent 1987, Stockholm, 1987.
- [43] Y. Li, S. Holmberg, L. Fuchs, Multi grid prediction of conjugate heat transfer and air flow in buildings, in: Proceedings of Building Simulation '93, Adelaide, Australia, International Building Performance Simulation Association, 16–18 August, 1993.
- [44] FLUENT V4.3 User's guide, in Fluent Inc. 1995.
- [45] N.C. Markatos, C.A. Pericleous, Laminar and turbulent natural convection in an enclosed cavity, in: Proceedings of the 21st National Heat Transfer Conference, Seattle, Washington, July 24–28, 1983.
- [46] R. Fauconnier, A. Grelat, P. Guillemard, Eléments d'analyse du régime dynamique en thermique du bâtiment, in: Rapport COSTIC, Fédération Nationale du Bâtiment, St Remy Les Chevreuses, 1989.
- [47] N. Markatos, C.A. Pericleous, Laminar and turbulent natural convection in an enclosed cavity, International Journal of Heat and Mass Transfer, 27(5) (1984) 755–772.
- [48] K. Limam, C. Inard, F. Allard, Etude expérimentale des transferts de masse and de chaleur à travers les grandes ouvertures verticales, Ventilation et renouvellement d'air, Gevra, Lyons, March, 1991.
- [49] J.-M. Nataf, F. Winkelmann, Symbolic modeling in building energy simulation. LBL Report LBL-35439, Lawrence Berkeley Laboratory, April, 1994.
- [50] J. Niu, J. van der Kooi, Dynamic simulations of combination of evaporative cooling with cooled ceiling system for office room cooling, in: Proceedings of Building Simulation '93, Adelaide, Australia, International Building Performance Simulation Association, 16–18 August, 1993.
- [51] H. Okuyama, Theoretical study on the building thermal network model (in Japanese). PhD thesis, Waseda University, December, 1987.
- [52] E.A. Rodriguez, S. Alvarez, I. Caceres, Prediction of indoor temperature and air flow patterns by means of simplified zonal models, in: Proceedings of ISES Solar World Congress, 1993, Budapest, Hungary, vol. 6, 1993.
- [53] E.A. Rodriguez, S. Alvarez, J.F. Coronel, Modelling stratification patterns in detailed building simulation codes, in: Proceedings of European Conference on Energy Performance and Indoor Climate in Buildings, 1994, Lyon, France, 24–25 November, 1994.
- [54] A. Setrakian, D. McLean, Building simulations using thermal and cfD models, in: Proceedings of Building Simulation '91, Sophia-Antipolis, Nice, France, International Building Performance Simulation Association, 20–22 August, 1991.
- [55] G. Shiralkar, A. Gadgil, C.L. Tien, High Rayleigh number convection in shallow enclosures with different end temperature, International Journal of Heat and Mass Transfer 24(19) (1981) 1621–1629.